Submitted, accepted and published by:
International Journal of Greenhouse Control 28 (2014) 168-179

Performance of Cu- and Fe-based oxygen carriers in a 500 W_{th} CLC unit for sour gas combustion with high H_2S content

L.F. de Diego[a,*], F. García-Labiano[a], P. Gayán[a], A. Abad[a], A. Cabello[a], J. Adánez[a], G. Sprachmann[b]

[a] Instituto de Carboquímica (ICB-CSIC), Department of Energy and Environment, Miguel Luesma Castán 4, Zaragoza 50018, SPAIN.

[b] Shell Global Solutions International BV. Amsterdam, The Netherlands.

* Corresponding author. Tel.: +34 976 733 977. Fax: +34 976 733 318. E-mail address: ldediego@icb.csic.es (Luis Francisco de Diego Poza)

Abstract

Sour gas represents about 43 % of the world's natural gas reserves. The sustainable use of this fossil fuel energy entails the application of CO_2 Capture and Storage (CCS) technologies. The Chemical Looping Combustion (CLC) technology can join the exploitation of the energy potential of the sour gas and the CO_2 capture process in a single step without the need of a sweetening pre-treatment unit. In this work, a total of 60 hours of continuous operation with sour gas and H_2S concentrations up to 15 vol. % has been carried out in a 500 W_{th} CLC unit, from which 40 corresponded to a Cu-based oxygen carrier (Cu14γAl) and 20 to a Fe-based

material (Fe20γAl). This is the first time that so high H_2S concentrations are present in a fuel to be burnt in a CLC process. The Cu14γAl oxygen carrier seems to be no recommendable for the combustion of sour gas because, although all the H_2S is burnt to SO_2, copper sulfides were formed at all combustion conditions. In contrast, the Fe20γAl oxygen carrier presented an excellent behavior with no agglomeration problems and maintaining the reactivity of the fresh material. The sour gas (CH_4, H_2, and H_2S) was completely burnt, and neither SO_2 was released in the AR nor iron sulfides were formed at usual CLC operating conditions. These tests demonstrated the possibility to use sour gas in a CLC process with 100% CO_2 capture without any SO_2 emissions to the atmosphere.

Keywords. CO_2 capture, Sour gas, Chemical Looping Combustion, oxygen carrier.

1. Introduction

Natural gas is a combustible mixture of hydrocarbon gases, being CH_4 the most abundant compound, usually between 70 to 90 vol.% . Other light hydrocarbons such as C_2H_6, C_3H_8 and C_4H_{10} are present in the gaseous mixture in variable concentrations up to 20 vol.%. This fuel gas is usually considered as sour gas if the H_2S content exceeds 5.7 milligrams of H_2S per cubic meter of natural gas (Katz et al., 1959), which is equivalent to approximately 4 ppm by volume under standard temperature and pressure. However, the composition of sour gas can vary widely depending on the extraction location, and wells with H_2S contents in the tens of percentage range are found (Hammer et al., 2006). According to Lallemand et al. (2012) a typical sour gas would contain about 10 vol.% H_2S, and high-sour and super-sour gases are considered those fuels with H_2S contents ≈ 20 vol.% and > 30 vol.%, respectively. Sour gas also contains significant amounts of other acid gas such as CO_2 that can reach contents higher than 10 vol.%. The presence of H_2S in natural gas poses Health and Safety Environmental (HSE) problems due to the high toxicity of H_2S which makes necessary special operating procedures to ensure

worker safety during drilling and in production operations. Furthermore, the presence of H_2S and CO_2 can affect negatively to the economic value of the gaseous fuel due to the additional costs required for special materials compatible with these corrosive compounds and for the natural gas sweeting unit necessary to remove them previous to commercialize the natural gas (Romano, 2007).

It is probed that the natural gas is continuously increasing its role in meeting the world energy demand. According to the International Energy Agency (IEA, 2013), about 43% of the world's natural gas reserves are sour gas sources, which revealed the great relevance of this type of fuel in the present and future energy scenario. The exploiting of the energy potential of sour gas entails the application of CO_2 Capture and Storage (CCS) technologies since the CO_2 content in this fuel can be appreciable as it was previously mentioned. Globally, the proven and probable sour gas resources have an estimated potential of 4 trillion m^3 of net natural gas and 15000 Mt of associated CO_2 (Burgers et al., 2011).

Direct combustion of sour gas with a high H_2S content produces a high SO_2 concentration in the flue gas. The separation of SO_2 from the other components of the flue gas implies significant costs due to the large volumes of gas to be treated, making this option economically not viable. Thus, H_2S should be removed from sour gas previously to its combustion. Usually, the process of H_2S removal from natural gas, i.e., the sweetening process, is usually performed by an amine gas treatment process (Maddox, 1974). The waste gas stream obtained from the sweetening process is commonly known as acid gas.

Because the removal of H_2S from natural gas requires additional expenses concerning extra units for acid gas enrichment, other novel technologies such as the Controlled Freeze Zone™ (CFZ) gas treatment technology (Parker et al., 2011) or Chemical Looping Combustion (CLC) have emerged in the last years as potential single step separation processes of CO_2, H_2S and other contaminants from a sour gas stream without the use of sorbents or absorbents.

The Chemical Looping Combustion technology would join the exploiting of the energy potential of the sour gas and the CO_2 capture process in a single step. Figure 1 shows the technology train to deal with sour gases through CLC.

CLC is a combustion technology based on the transfer of oxygen from air to fuel by means of a solid oxygen carrier which is continuously circulating between two interconnected fluidized bed reactors, the air reactor (AR) and the fuel reactor (FR) (Adánez et al., 2012). When a carbonaceous fuel is considered to be burnt, in a first step the fuel is oxidized in the FR to CO_2 and H_2O by a metal oxide (Me_xO_y) which is reduced to a metal (Me) or reduced form (Me_xO_{y-1}). A highly concentrated stream of CO_2 is obtained after water condensation and purification. In a second step, the metal or reduced metal oxide is oxidized with air in the AR regenerating the material for a new cycle.

The objective in a CLC process that uses sour gas as fuel is to generate a highly concentrated stream of CO_2 and SO_2 in the FR, avoiding as much as possible the release of sulfur in the AR stream. The SO_2 produced in the FR can be separated at a lower cost since the volumetric flow of the flue gases is seven times less than by means of direct combustion in the burner-boiler, resulting in significantly smaller post-treatment units. Shell Global Solutions International BV company has developed a patent (Mirfenderski and Sprachmann, 2013) where sour gas is used as fuel for thermal energy conversion without the need of a sweetening pre-treatment utilizing the high caloric content of burning H_2S, with improved capture of the produce SO_2, whilst maintaining the CO_2 inherent separation characteristics of CLC. The captured SO_2 may be sent to a next destination such as e.g. a sulfuric acid plant, a sulfur recovery plant, liquid SO_2, or even injection of the CO_2/SO_2 mixture.

The selection of the oxygen carrier for a particular CLC process depends on the type of fuel, the operating conditions to be adopted, the cost and the lifetime of the material, environmental aspects, etc. In addition, the resistance to sulfur is a crucial aspect to be considered when sour gas is used. ICB-CSIC research group studied the behavior of four highly reactive oxygen carriers in a 500 W_{th} continuous CLC unit regarding the presence of H_2S in the gaseous fuel. These oxygen carriers were based on Ni (García-Labiano et al., 2009), Mn (Cabello et al., 2014b), Fe (Cabello et al., 2014a) and Cu (Forero et al., 2010) oxides. The material based on nickel oxide was not suitable to be used for the CLC process with H_2S-containing fuels, at concentrations higher than 100 vppm, since deactivation of the oxygen carrier took place at all

operating conditions by Ni_3S_2 formation. Regarding the Mn-based oxygen carrier, in the form of a perovskite ($CaMn_{0.9}Mg_{0.1}O_{3-\delta}$), the addition of H_2S caused a negative effect on its behavior for the CLC process in terms of agglomeration problems, deactivation and loss of oxygen uncoupling capacity. Thermodynamic analyses conclude that manganese sulfides are not found as predominant sulfur species during the interaction of Mn-based oxygen carriers with sulfur (Jerndal et al., 2006; Wang et al., 2005). The poisoning of this perovskite by H_2S addition was not due to the presence of manganese oxide within its structure, but due to the presence of Ca that could form certain undesired compounds such as $CaSO_4$ and CaS.

Fe- and Cu-based oxygen carriers presented a good CLC performance using fuels containing H_2S (Cabello et al., 2014a; Forero et al., 2010). In the case of the Fe-based oxygen carrier, the presence of H_2S in the fuel gas did not affect the behavior of the material independently of the amount of sulfur present in the fuel stream. Iron sulfides were not formed, the redox reactivity was maintained during operation and high combustion efficiencies were obtained with and without sulfur presence. Regarding the Cu-based oxygen carrier, the presence of H_2S did not produce the deactivation of the material working at oxygen carrier-to-fuel ratios, ϕ, above 1.5. At these conditions, complete combustion of fuel was achieved and the great majority of the sulfur fed into the system ($\approx$ 95 vol. %) was released in the gas outlet stream of the FR as SO_2. For ϕ values lower than 1.5, the formation of copper sulfide, Cu_2S, was detected, and the oxygen carrier was deactivated. However, this material was completely regenerated in a H_2S-free atmosphere.

It must be remarked that the maximum H_2S content in all the above works was 3400 vppm. However, the amount of H_2S in sour gas sources can be very elevated, being increased several orders of magnitude (Katz et al., 1959). As above mentioned, the composition of sour gas can vary widely depending on the extraction location, and wells with H_2S contents in the tens of percentage range can be found (Hammer et al., 2006; Lallemand et al., 2012). The presence of sulfur in the fuel can affect to the quality of the concentrated CO_2 stream obtained or to the admissible emission of pollutants if it is released as SO_2 in the FR or AR, respectively. In

addition, the possible poisoning of the oxygen carrier by sulfur becomes crucial when using sour gas as fuel because metal sulfides formation decreases the oxygen carrier reactivity, oxygen transport capacity and fuel conversion potential.

Based on previous experience, the objective of this work was to analyze the behavior of two materials based on Cu and Fe, respectively, during sour gas combustion in a 500 W_{th} CLC unit in presence of high H_2S concentrations, up to 15 vol. %. The influence of H_2S concentration on the gas products distribution, sulfur splitting between FR and AR and oxygen carrier deactivation were investigated. Furthermore, the evolution of the main oxygen carrier properties during the time of operation was also analyzed.

2. Experimental section

2.1 Oxygen carrier materials

A Cu- and a Fe-based oxygen carriers were prepared at ICB-CSIC by the incipient impregnation method using γ-Al_2O_3 as support. These materials were designated as Cu14γAl and Fe20γAl oxygen carrier respectively. The CuO content in the Cu14γAl oxygen carrier particles was 14.2 wt.%, whereas the Fe_2O_3 content in the Fe20γAl material was 20.4 wt.%. The corresponding oxygen transport capacities, R_{OC}, were 2.9 and 2.0 %, respectively. The method of preparation and the main physical and chemical properties of both materials were deeply explained by Adánez et al. (2006) and Gayán et al. (2012).

2.2 ICB-CSIC-g1 facility

Sour gas combustion tests were carried out in the ICB-CSIC-g1 facility (500 W_{th}). Figure 2 shows a schematic diagram of the unit after the modifications made for safe operation with high H_2S concentrations. The atmospheric chemical-looping combustor prototype was composed of two interconnected fluidized-bed reactors, the air reactor and the fuel reactor, separated by a loop seal, a riser for solids transport to the fuel reactor, a cyclone and a solid valve to control the solids fed to the fuel reactor. An important feature of the prototype was the possibility to control and measure the solids circulation rate at any moment through the solids valves located above

164 the FR. Moreover, the prototype allowed the collection of solid material samples from the AR
165 or the FR at any moment for further characterization. A detailed description of the installation
166 can be found elsewhere (García-Labiano et al., 2009; Forero et al., 2010).
167 The CLC unit was modified by including three mass flow controllers for H_2S, H_2 and H_2O. The
168 synthetic sour gas was fed at the bottom of the reactor. This made necessary the use of a special
169 distributor plate manufactured in Kanthal APM. H_2 was also added to avoid H_2S decomposition
170 in the feeding line. Furthermore, to avoid corrosion problems with reactor alloys some steam
171 was also included in the feeding gas stream. Two scrubbers containing a saturated solution of
172 sodium carbonate were located in the gas outlet streams of the FR and AR reactors to keep the
173 emissions below the Health, Safety and the Environment (HSE) limits. Furthermore, a special
174 installation for gas leakage detection was included in the CLC unit. This security system is
175 composed by three gas detectors, a control unit and two electronic valves. Two gas detectors
176 (one for H_2S and another one for SO_2) were located inside the cupboard covering the CLC plant,
177 and an additional H_2S gas detector was installed outside near the plant. The gas detectors were
178 configured for 5 vppm alarm. All the detectors were connected to the control unit. If a gas
179 leakage was detected, several alarms were switched on and the relays of the control unit acted
180 on the electronic valves. In such case, the H_2S flow was closed and the line was flushed with N_2.
181 Some specific analyzers for sulfur compounds were placed at the outlet streams of the AR and
182 FR. A non-dispersive infrared (NDIR) analyzer (Siemens Ultramat U22) was used to detect the
183 SO_2 concentration obtained at the AR gas outlet stream. Different solutions were used for on-
184 line gas concentration determination downstream the FR: a) a NDIR analyzer to measure the
185 SO_2 concentration, and b) a gas chromatograph (Varian 3400-CX GC) equipped with a
186 PORAPAK-Q packed column and a sulfur-specific Flame Photometric Detector (FPD) for the
187 SO_2 determination at low concentrations, and with a Thermal Conductivity Detector (TCD) for
188 SO_2 concentrations above 1 vol.%. In this way, it was also possible the detection of the different
189 gaseous sulfur compounds that can appear in the FR such as H_2S, SO_2, COS, CS_2, etc. The
190 chromatograph was calibrated in the range 0-2000 vppm for H_2S and 0-20 vol. % for SO_2. It
191 must be remarked that only the SO_2 concentration data corresponding to the NDIR analyzer will

be showed in Section 3 of this paper. Furthermore, the sulfur mass balances that appear in Sections 3.1.3 and 3.2.3 were carried out considering the aforementioned data.

2.3 Testing conditions

The total solids inventory in the system was the same for both oxygen carriers, 1.2 kg approximately, of which 0.3 and 0.5 kg were in the FR and AR, respectively. A total operation time of 60 hours of continuous operation with sour gas and different H_2S concentrations up to 15 vol. % were carried out in the 500 W_{th} CLC unit, from which 40 hours corresponded to the Cu-based oxygen carrier and 20 hours to the Fe-based material. The temperatures used in the CLC unit were different for the sour gas combustion tests depending on the oxygen carrier used. In the case of the Cu14-γAl material, the temperatures in the FR and AR were 1073 K and 1123 K respectively. On the other hand, the Fe-based oxygen carrier was subjected to higher temperatures: 1173 K in the FR and 1223 K in the AR. The gas flows fed to the reactors were identical for all sour gas combustion tests. The inlet gas flow in the FR was 191 L_N/h (0.1 m/s at 1173 K). The AR was fluidized with air, which was divided into the primary air, added from the bottom bed (720 L_N/h), and the secondary air, added at the top of the bubbling bed to help particle entrainment in the riser (150 L_N/h). Nitrogen was also used to fluidize the bottom loop seal (37.5 L_N/h).

Tables 1 and 2 shows a summary of the main variables used in the sour combustion tests carried out with the Cu-based and Fe-based materials respectively. The oxygen carrier-to-fuel ratio, ϕ, which was defined as the ratio between the oxygen supplied and the oxygen needed to stoichiometrically react with the fuel flow, was calculated by Eq. (1) as follows:

$$\phi = \frac{F_{MeO}}{b \cdot F_{Fuel}} \quad (1)$$

where F_{MeO} is the molar flow rate of the metal oxide. F_{MeO} can be calculated considering both the solid flow rate (measured by means of a diverting solids valve located below the cyclone, see Figure 2) and the metal oxide content of the oxygen carrier. F_{Fuel} is the inlet molar flow rate of the fuel in the FR. The parameter b is the stoichiometric coefficient of the fuel gas and depends on the oxygen carrier used during combustion tests (Cu-based or Fe-based oxygen

219 carrier) and on the fuels present in the sour gas composition (CH_4, H_2S, and H_2). This parameter
220 was determined as a function of the solids circulation rate, f_s. A value of $\phi = 1$ corresponds to
221 the stoichiometric MeO amount needed for complete conversion of the sour gas to CO_2, SO_2,
222 and H_2O.
223 Regarding the combustion tests conducted with the Cu14-γAl material, test Cu1 corresponded to
224 the reference test carried out without H_2S addition. Tests Cu2-Cu4 were performed the first days
225 of operation with sulfur addition. During these tests, the H_2S concentration was low, reaching
226 values up to 3 vol. %. Tests Cu5-Cu6, Cu7-Cu9 and Cu10-Cu12 corresponded to H_2S
227 concentrations of 5, 10 and 15 vol. %, respectively. For each H_2S concentration tested in the
228 CLC unit, several CH_4 contents were used. The variation of concentration of both compounds
229 allowed us to check the behavior of the oxygen carrier under different oxygen carrier-to-fuel
230 ratios. At the end of the experimentation, a total of 40 hours of continuous operation with H_2S
231 feeding was reached.
232 Finally, test Cu13 was carried out with a new batch of oxygen carrier particles selecting the
233 same operating conditions as in test Cu5, but replacing N_2 for CO_2 as gas balance. This
234 atmosphere would better represent the atmosphere existing in a FR where only fuel is added. It
235 must be remarked that the CLC unit of ICB-CSIC is limited by the AR design up to 500 W_{th}.
236 This fact makes necessary to use some gas as balance that it is introduced together with the fuel.
237 In the case of the Fe-based oxygen carrier, most of the tests were carried out using CO_2 as
238 diluting agent. Tests Fe1-Fe4 corresponded to experiments with 10 vol.% CH_4, 5 vol.% H_2 and
239 increasing amounts of H_2S from 0 up to 15 vol.%. Tests Fe5-Fe8 were carried out at a higher
240 CH_4 content (20 vol.%) and increasing amounts of H_2S (up to 15 vol.%). It must be remarked
241 that in tests Fe7 and Fe8 the ϕ value was very low. After that, it was decided to repeat test Fe6
242 in order to check if repetitive results were obtained. Finally, tests Fe10 and Fe11 were
243 performed at the same operating conditions as in tests Fe6 and Fe1, but replacing the CO_2 gas
244 balance by N_2. These last tests were carried out to check again if the variation of gas affected to

245 the obtained results. At the end, 20 hours of continuous operation were performed with the
246 Fe20γAl oxygen carrier.
247
248 **3. Results**
249 **3.1 Tests of sour gas combustion with the Cu14-γAl oxygen carrier**
250 **3.1.1 Thermodynamic calculations for copper materials**
251 A thermodynamic study was carried out using the HSC Chemistry 6.1 (2008) software to
252 determine the fate of sulfur when Cu-based oxygen carriers are used in a CLC plant with sour
253 gas. This program obtains the equilibrium composition by using the method of minimization of
254 the Gibbs free energy of the system for a fixed mass balance, at constant pressure and
255 temperature.
256 The calculations were performed considering CuO as oxygen carrier and typical sour gas
257 compositions. Figure 3 shows the thermodynamic equilibrium of the compounds existing in the
258 FR for two sour gas compositions, (sour gas 1: 99.5 vol.% CH_4 - 0.5 vol.% H_2S, and sour gas 2:
259 85 vol.% CH_4 - 15 vol.% H_2S) as a function of the oxygen carrier-to-fuel ratio, ϕ, and at 1073 K.
260 The reactions considered between the fuel (CH_4 + H_2S) and the active phase of the oxygen
261 carrier are the following depending on the value of parameter ϕ:

262 $8\ CuO + CH_4 \Leftrightarrow 4\ Cu_2O + CO_2 + 2\ H_2O \qquad (\phi > 2)$ (2)

263 $4\ Cu_2O + CH_4 \Leftrightarrow 8\ Cu + CO_2 + 2\ H_2O \qquad (2 > \phi > 1)$ (3)

264 $6\ CuO + H_2S \Leftrightarrow 3\ Cu_2O + SO_2 + H_2O \qquad (\phi > 2)$ (4)

265 $3\ Cu_2O + H_2S \Leftrightarrow 6\ Cu + SO_2 + H_2O \qquad (2 > \phi > 1)$ (5)

266 The values obtained from the thermodynamic analysis were expressed as the volumetric
267 percentage of gas product composition for sour gas combustion and as the molar percentage of
268 sulfur species present in the products in relation to the sulfur fed into the system. At ϕ values
269 above 1, complete combustion of fuel gas to CO_2, H_2O and SO_2 was achieved (see Equations 2
270 – 5). The unique stable sulfur compound at these conditions was SO_2. If the oxygen carrier-to-
271 fuel ratio decreased below 1, unreacted H_2 and CO appeared and reached a maximum when H_2O

and CO_2 concentrations are zero. Below that point, CH_4 appeared as an unreacted gas. Moreover, different solid and gaseous sulfur species, mainly Cu_2S and H_2S, appeared at sub-stoichiometric conditions as a function the oxygen present in the system. The concentration of H_2S and Cu_2S in equilibrium depended on the H_2 concentration through reaction (6):

$$2\ Cu + H_2S \Leftrightarrow Cu_2S + H_2 \quad (6)$$

It can be observed that the amount of Cu_2S in equilibrium increased with the H_2S content in the sour gas. Thermodynamic calculations made at different temperatures from 973 to 1273 K showed similar results.

The above results were obtained considering CuO as the only active copper-based specie present in the oxygen carrier particles. However, XRD characterization showed that Cu14-γAl material was composed by CuO and a spinel-structure $CuAl_2O_4$ due to the interaction between the active phase (CuO) and support (γ-Al_2O_3) (Adánez et al., 2006). The distribution between CuO and $CuAl_2O_4$ in the oxygen carrier depends on several factors but the presence of $CuAl_2O_4$ can be as high as 75 % during usual operation. Experience on previous works carried out at ICB-CSIC indicated that both compounds were able to react with fuel gases, i.e., the spinel phase was also reducible by the fuel gas (de Diego et al., 2004, 2005, 2007).

The reduction reactions that take place in the FR between $CuAl_2O_4$ and the combustible fraction of sour gas are the following:

$$8\ CuAl_2O_4 + CH_4 \Leftrightarrow 8\ CuAlO_2 + 4\ Al_2O_3 + CO_2 + 2\ H_2O \quad (\phi > 2) \quad (7)$$

$$8\ CuAlO_2 + CH_4 \Leftrightarrow 8\ Cu + 4\ Al_2O_3 + CO_2 + 2\ H_2O \quad (2 > \phi > 1) \quad (8)$$

$$6\ CuAl_2O_4 + H_2S \Leftrightarrow 6\ CuAlO_2 + 3\ Al_2O_3 + SO_2 + H_2O \quad (\phi > 2) \quad (9)$$

$$6\ CuAlO_2 + H_2S \Leftrightarrow 6\ Cu + 3\ Al_2O_3 + SO_2 + H_2O \quad (2 > \phi > 1) \quad (10)$$

The oxidation in the AR happens through reactions (11) and (12):

$$2\ Cu + 1/2\ O_2 + Al_2O_3 \Leftrightarrow 2\ CuAlO_2 \quad (11)$$

$$2\ CuAlO_2 + 1/2\ O_2 + Al_2O_3 \Leftrightarrow 2\ CuAl_2O_4 \quad (12)$$

The same thermodynamic calculations as in the previous case with CuO were performed considering $CuAl_2O_4$ as oxygen carrier. In this case $CuAl_2O_4$ data given from Jacob and Alcock

299 (1975) were used to carry out the thermodynamic analyses. The obtained results were identical
300 with both Cu-based compounds, CuO and $CuAl_2O_4$, as it can be observed in Figure 3.

301 **3.1.2 Combustion tests in the ICB-CSIC-g1 facility**

302 To evaluate the suitability of the Cu14-γAl material for sour gas combustion, some experimental
303 tests were performed in the $500W_{th}$ CLC unit. The combustion efficiency, the sulfur splitting
304 between reactors, and the reactivity of fresh and after-used particles were analyzed for each
305 experiment.

306 In test Cu1, without H_2S addition, full combustion of CH_4 to CO_2 and H_2O was obtained. This is
307 the usual behavior of this Cu-based material at the operating conditions used here. The absence
308 of carbon formation in the oxygen carrier particles was maintained during the whole
309 experimentation.

310 During the first 2 hours of operation with sulfur addition (3000 vppm) in test Cu2, no SO_2 was
311 detected at the outlet gas stream of the FR or AR. After that, almost all the sulfur fed to the
312 installation was detected as SO_2 at the gas outlet stream from the FR.

313 During tests Cu3 and Cu4, CH_4 was fully burnt to CO_2 and H_2O. CO, H_2, and H_2S were never
314 detected in the FR stream. The latter compound was mainly transformed into SO_2 through
315 reactions (4), (5), (9) and (10). In addition, variable amounts of SO_2 (up to 300-400 vppm) were
316 found at the outlet of the AR.

317 During tests Cu5 and Cu6, with a sulfur content of 5 vol.% H_2S in the feeding gas, the SO_2
318 concentration at the outlet gas stream from the FR was maintained quite constant during all the
319 operation time with values close to the sulfur fed. However, the amounts of SO_2 detected at the
320 outlet of the AR increased, reaching values up to 2000 vppm (5720 mg/Nm^3) in test Cu5. In test
321 Cu6, CH_4 concentration was decreased, which corresponded to an increase in the value of the
322 parameter ϕ. The response to this change in the gas product distribution was very quick in both
323 reactors, with slightly increasing the SO_2 concentration in the FR and decreasing in the AR up
324 to values of 100-200 ppm (286-572 mg/Nm^3). To corroborate if this change could be attributed
325 to the change in the value of ϕ, the conditions of test Cu5 were again reestablished, and the

previous values were again reached. This fact demonstrated a relation between the oxygen carrier-to-fuel ratio and the SO_2 concentration obtained at the outlet of the AR, in such a way that the SO_2 concentration was higher as lower was the ϕ value. A similar behavior was found when the solids circulation rate was varied.

A possible explanation to this phenomenon may be that some Cu_2S was formed inside the FR through reaction (6), being favored when more metallic copper was present in this reactor, that is, when the circulation rate or the ϕ value were lower. The Cu_2S transported to the AR could be partially burnt to SO_2 according to reaction (13):

$$Cu_2S + 2\ O_2 \Leftrightarrow 2\ CuO + SO_2 \qquad (13)$$

As an example of the sour gas combustion tests, Figure 4 shows the gas composition obtained at the outlet of the FR and AR for the tests Cu7-Cu9 corresponding to 10 vol.% H_2S in the gas feeding. It was observed the same relation between parameter ϕ and the SO_2 concentration obtained at the outlet of the AR as in tests Cu5 and Cu6, i.e., the SO_2 concentration was higher as lower was the value of the parameter ϕ. Again, it was possible that some Cu_2S could be formed in the lower zone of the fluidized bed, which was partially released in the AR as SO_2 and some was being accumulated in the particles.

In the lower part of Figure 4 a graph showing the instantaneous sulfur mass balance was added. This mass balance, expressed as mol of sulfur per hour, includes the sulfur fed to the system, the sulfur detected at the outlet of the FR and AR, and the total sulfur in the gas phase leaving both reactors. The difference between the sulfur fed and the total sulfur detected in the gas phase at the exit of the FR and AR could be due to experimental errors or to formation of copper sulfides in the oxygen carrier particles.

In the experimental tests Cu10-Cu12 performed with the highest concentration of H_2S, i.e., 15 vol.%, it was found again the same relation between the SO_2 released in the AR and the parameter ϕ. However, these tests showed the lowest emissions of sulfur in the gas phase among all the tests, which indicated that there were more sulfides formed or more experimental errors in the measurements. It must be considered that tests Cu10-Cu12 correspond to the most

353 extreme conditions, with the highest H_2S concentration, and when the particles have already
354 been subjected to almost 40 hours of continuous operation with some sulfur accumulated inside
355 the particles, as it will be showed later (see Section 3.1.4). Nevertheless, agglomeration was
356 never detected in the CLC unit using this oxygen carrier. The presence of sulfur inside the
357 particles did not alter their properties regarding agglomeration because they were prepared
358 under the guidelines proposed by de Diego et al. (2005) to avoid this problem in copper-based
359 oxygen carriers.
360 After test Cu12, the whole solids inventory was replaced by a new batch of particles and an
361 additional test, test Cu13, was carried out at the same operating conditions as in test Cu5 but
362 using CO_2 instead of N_2 as gas balance. This test was performed to analyze the effect of the
363 reacting atmosphere on the behavior of the oxygen carrier during sour gas combustion. The
364 results obtained in terms of gas product distribution and sulfur mass balance were similar to the
365 obtained in test Cu5 which indicated that the gas balance atmosphere had a negligible effect on
366 the material performance.

367 **3.1.3 Sulfur mass balance**

368 A sulfur mass balance was performed to the different tests carried out in the CLC unit with the
369 Cu14γAl material. Sulfur splitting between reactors and the possible formation of copper
370 sulfides in the oxygen carrier particles were analyzed. Figure 5 shows this balance in terms of
371 percentage of sulfur released in both FR and AR. It can be observed that most of the sulfur
372 appeared as SO_2 in the FR, and a minor part (less than 13 wt.%) in the AR. It can be also
373 noticed that there was an amount of sulfur that was not detected in the gas phase. This amount
374 was high in some tests, which cannot be only attributed to experimental errors. It was concluded
375 that some sulfur was accumulated in the oxygen carrier, as it will be demonstrated in the next
376 characterization section. It must be remarked the behavior of the material during the first
377 experiment with sulfur addition (test Cu2), where there was an important accumulation of sulfur
378 inside the oxygen carrier particles since only a 23 % of the sulfur fed was released as SO_2 in the
379 FR. Also, it is remarkable the results obtained in tests Cu10-12 which presented the lowest
380 sulfur emissions in the gas phase, both in FR and AR. These tests correspond to the most

381 extreme conditions, with the highest H_2S concentration, and after 35 hours of continuous
382 operation.
383 According to the thermodynamic data showed in section 3.1.1, and considering that the tests
384 were always carried out at ϕ values above 1, no copper sulfides should be formed at any of the
385 operating conditions used during the experimental work. However, it is necessary to take into
386 consideration that inside the FR fluidized bed could be a reducing zone with possible high CO
387 and H_2 concentrations and considerable presence of metallic copper that could be responsible of
388 the copper sulfides formation (Forero et al., 2010), see reaction (6). To confirm this possibility,
389 a solid characterization to samples extracted from the system at different times was carried out.

390 **3.1.4 Characterization of the oxygen carrier**

391 Samples of Cu14γAl material were extracted from the FR and AR at the end of each
392 experimental test for solid characterization. Table 3 shows the main characteristics of those
393 samples.
394 XRD characterization showed the main compounds existing in the samples extracted from the
395 AR. The equipment used was a X-ray diffractometer Bruker AXS D8 Advance with Bragg-
396 Brentano geometry configuration, Cu Kα radiation and equipped with secondary graphite
397 monochromator. Different crystalline species, such as Al_2O_3, $CuAl_2O_4$ and CuO, were detected.
398 Regarding stable sulfur phases, no copper sulfides were detected in any case. However, it is
399 reasonable to think that the amounts of copper sulfides were below the detection limit of the
400 apparatus (5 wt.%). To check the presence of sulfur in the oxygen carrier particles at lower
401 amounts, the samples were analyzed by ultimate analysis in a Thermo Flash 1112. From this
402 characterization technique, important amounts of sulfur were detected, which are showed in
403 Table 3. Considering Cu_2S as the unique copper sulfide possible at the experimental conditions
404 used in the tests, the content of this compound in the samples was calculated. It seems that the
405 Cu_2S content depends on the operation conditions and it can be concluded that sulfur was being
406 accumulated along time in the oxygen carrier particles during the sour gas combustion tests.
407 The presence of sulfur inside the particles was also detected by SEM-EDX. The equipment used
408 was a scanning electron microscope (SEM) ISI DS-130 coupled to an ultra-thin window PGT

409 Prism detector for energy-dispersive X-ray (EDX). Figure 6 illustrates a SEM image of a cross-
410 section of an oxygen carrier particle after 40 h of sour gas combustion inside the CLC
411 prototype. It can be observed that a significant presence of sulfur was detected in those areas
412 where metallic copper was accumulated.
413 Finally, the reactivity of the oxygen carrier particles along the time of operation was determined
414 in a TGA CI Electronics type, described elsewhere (Abad et al, 2011), using CH_4 as reducing
415 gas. It was observed in Figure 7 that samples lost some oxygen transport capacity and reactivity.
416 Nevertheless, the reactivity until 40 % of solid conversion was maintained high. In this point it
417 must be highlight that the ϕ values used in the CLC unit were in the range from 1.3 to 3.7,
418 corresponding to variations of solid conversion below 0.6 in most of the experiments. By this
419 reason, a decrease in the CH_4 conversion along time was not noticed during combustion tests.
420 However, it is expected that reactivity decreases below acceptable values for long operating
421 times as the existing in CLC units at industrial scale. The SO_2 concentrations at the outlet of the
422 AR corresponded to values measured at the operating conditions used in the tests. When these
423 values were normalized to an excess of 6 vol.% O_2, the SO_2 emissions were always higher than
424 200 mg/Nm^3, the EU emissions limit for boilers higher than 200 MW_{th}. Considering the above
425 data and the confirmed accumulation of sulfur in the oxygen carrier particles as Cu_2S, the use of
426 Cu-based oxygen carriers for sour gas combustion with high H_2S concentrations is not
427 recommended.

428 **3.2 Tests of sour gas combustion with the Fe20γAl oxygen carrier**

429 **3.2.1 Thermodynamic calculations for iron materials**

430 Similar calculations to the previously ones were performed for Fe-based materials.
431 Thermodynamic calculations of different sour gas compositions were carried out in a range of
432 temperature from 1073 K to 1373 K. Figure 8a shows the thermodynamic equilibrium existing
433 at 1223 K, for a sour gas composed by 85 vol.% CH_4 and 15 vol.% H_2S, as a function of the
434 oxygen carrier-to-fuel ratio, ϕ, when the redox pair considered is Fe_2O_3-Fe_3O_4. In this case, a

435 value of ϕ = 1 corresponds to the stoichiometric amount of Fe_2O_3 needed for a full conversion of
436 the fuel (CH_4+H_2S) to CO_2, SO_2, and H_2O through reactions (14) and (15).

437 $$12\ Fe_2O_3 + CH_4 \Leftrightarrow 8\ Fe_3O_4 + CO_2 + 2\ H_2O \quad (14)$$

438 $$9\ Fe_2O_3 + H_2S \Leftrightarrow 6\ Fe_3O_4 + SO_2 + H_2O \quad (15)$$

439 Thermodynamic results are expressed as the volumetric percentage of gas composition and as
440 the molar percentage of sulfur species present in the products in relation to the sulfur fed into
441 the system. Furthermore, Figure 8a includes the different iron species in equilibrium at the
442 different ϕ values considered. At ϕ values above 1, complete combustion of the fuel gas mixture
443 to CO_2, H_2O, and SO_2 was achieved. Again, the unique stable sulfur compound working with
444 Fe-based oxygen carriers was SO_2, similarly to the case with the Cu-based oxygen carrier. At
445 sub-stoichiometric conditions, CO_2 and H_2O concentrations decreased as the amount of oxygen
446 provided by the active Fe-based specie was reduced. On the contrary, H_2 and CO concentrations
447 progressively increased reaching their maximum values when the iron oxide was fully reduced
448 to metallic iron. Finally, at very low ϕ values, lower than 0.1, unreacted CH_4 appeared in the
449 equilibrium while the amounts of CO and H_2 dramatically decreased. Different solid and
450 gaseous sulfur species can appear at ϕ values below 1 depending on the oxygen available in the
451 system. The main iron sulfide present was the $Fe_{0.877}S$ and always appeared some H_2S in
452 equilibrium. Small amounts of S_2 (g) were also found at ϕ values close to 1.
453 However, a special case corresponds to Fe-based oxygen carriers prepared by impregnation on
454 Al_2O_3. In this case, iron aluminate ($FeAl_2O_4$) can be formed as reduced compound allowing
455 complete combustion of gas to CO_2 and H_2O (Abad et al., 2007; Cabello et al., 2014a; Gayán et
456 al., 2012; Leion et al., 2008), and increasing three times the oxygen transport capacity of the
457 oxygen carrier in comparison with the redox pair Fe_2O_3-Fe_3O_4. Additional thermodynamic
458 calculations including Al_2O_3 as solid phase were performed using the HSC Chemistry 6.1
459 program. Figure 8b shows the results corresponding to sour gas containing 15 vol.% H_2S. In this
460 case, a value of ϕ = 1 corresponds to the stoichiometric amount of Fe_2O_3, supported on Al_2O_3,

needed for full conversion of the fuel (CH_4+H_2S) to CO_2, SO_2 and H_2O when the redox pair considered is Fe_2O_3 (Al_2O_3) - $FeAl_2O_4$.

$$4\ Fe_2O_3 + 8Al_2O_3 + CH_4 \Leftrightarrow 8\ FeAl_2O_4 + CO_2 + 2\ H_2O \quad (16)$$

$$3\ Fe_2O_3 + 6Al_2O_3 + H_2S \Leftrightarrow 6\ FeAl_2O_4 + SO_2 + H_2O \quad (17)$$

The gas product distribution and the sulfur species at ϕ values higher than 1 were the same as in the previous case when the redox pair Fe_2O_3- Fe_3O_4 was considered: full combustion of fuel gas to CO_2, H_2O, and SO_2 as the unique sulfur compound present in the system. At sub-stoichiometric conditions, unreacted H_2 and CO appeared reaching their maximum values when the equilibrium Fe-$FeAl_2O_4$ was found. In this case, CO_2 and H_2O were not present in the gas equilibrium. CH_4 appeared as an unreacted gas at very low ϕ values when hematite was fully reduced to metallic iron. Interesting results were obtained at sub-stoichiometric conditions regarding sulfur species present in the reaction products. In this case, formation of iron sulfides were only possible at very low values of ϕ (ϕ<0.4), with most of the sulfur appearing as H_2S. This can be considered as a remarkable result and even more if we consider that the transformation Fe_2O_3 (Al_2O_3) - $FeAl_2O_4$ supposes to increase three times the oxygen transport capacity with respect to the use of the pair Fe_2O_3-Fe_3O_4. Thermodynamic calculations made at temperatures from 1073 to 1373 K and sour gas with different H_2S contents showed similar results.

3.2.2 Combustion tests in the ICB-CSIC-g1 facility

The behavior of the Fe-based oxygen carrier in sour gas atmospheres with high H_2S concentrations was analyzed in the ICB-CSIC-g1 facility under continuous operating conditions. Table 2 shows the combustion tests carried out and the experimental conditions used.

During tests Fe1-Fe4, with a CH_4 concentration of 10 vol.%, neither CO nor H_2 was detected in the gas outlet stream from FR and full combustion of CH_4 to CO_2 and H_2O was obtained with 100 % of carbon capture. Reactions (16) and (18) were considered to take place in the FR:

$$Fe_2O_3 + 2\ Al_2O_3 + H_2 \Leftrightarrow 2\ FeO{\cdot}Al_2O_3 + H_2O \quad (18)$$

In addition, neither CO nor CO_2 was detected in the AR in any of the tests, which means that no carbon was ever formed during fuel combustion in the FR. In the AR, the oxidation of the material took place through reaction (19):

$$8\ FeAl_2O_4 + 2\ O_2 \Leftrightarrow 4\ Fe_2O_3 + 8\ Al_2O_3 \quad (19)$$

Taking into account the results of previous works (Cabello et al., 2014, Gayán et al., 2012), this is the usual behavior of this Fe-based material at the operating conditions used when no H_2S was fed into the combustor.

Regarding the combustion of the H_2S fed to the CLC system during tests Fe2-Fe4, it must be remarked the very good behavior obtained with this oxygen carrier. All the H_2S was burnt by the oxygen carrier through reaction (17) and the SO_2 concentration obtained at the outlet of the FR was very close to the one corresponding to full combustion of H_2S. No SO_2 was released in the AR in any of the operating conditions.

Due to the excellent results obtained in tests Fe1-4, the CH_4 concentration was increased up to 20 vol.% in tests Fe5-Fe9 to analyze the oxygen carrier behavior when the parameter ϕ took lower values (see Table 2). The results obtained in these tests are showed in Figure 9.

Test Fe5 corresponded to the reference test without H_2S addition and a CH_4 concentration of 20 vol.%. In this case, the combustion of CH_4 was almost complete because a very small amount of unreacted CH_4 (< 0.8 vol.%) appeared at the outlet stream from the FR. Furthermore, neither H_2 nor CO was detected. During test Fe6, full H_2S combustion to SO_2 and almost full combustion of CH_4 to CO_2 and H_2O was achieved in the FR. However, an increase in the H_2S concentration up to 15 vol.% (test Fe8) produced a decrease in the percentage of SO_2 obtained in the FR in relation to the H_2S fed. Furthermore, some unconverted CH_4 appeared in the FR and increasing amounts of SO_2 appeared in the AR. This last fact could be as a consequence of the iron sulfides formed in the FR through reaction (20) that could be burnt in the AR according to reaction (21) due to the low ϕ values (1.5 and 1.3, respectively) used in these tests.

$$FeO{\cdot}Al_2O_3 + H_2S \Leftrightarrow FeS + Al_2O_3 + H_2O \quad (20)$$

$$2\ FeS + 7/2\ O_2 \Leftrightarrow Fe_2O_3 + 2\ SO_2 \quad (21)$$

As it was mentioned in Section 3.2.1, thermodynamic calculations showed that $Fe_{0.877}S$ was the only stable sulfide that could be formed at ϕ values lower than 0.4, through the reaction (20). Nevertheless, in order to facilitate the adjustment of the chemical reactions, FeS has been considered as the stable iron sulfide instead of the $Fe_{0.877}S$ compound.

Comparing the ϕ values needed to boost thermodynamically the formation of iron sulfides with the ones used in the CLC plant during the experimental campaign, it could be concluded that iron sulfides should be not formed in any case at usual operating conditions.

After that, conditions corresponding to test Fe6 were reestablished in test Fe9 to evaluate if iron sulfides were reversible when the amount of oxygen available for combustion increased. In this case, CH_4 concentration at the outlet of the FR decreased, i.e., the combustion behavior of the oxygen carrier particles was improved, and more sulfur, in the form of SO_2, was detected at the outlet of the FR in relation to the amount fed into the CLC system. These results indicated that the possible iron sulfides formed at reducing conditions were reversible and no accumulation in the particles was produced. The regeneration of the iron sulfides would be carried out in the FR by the reverse of reaction (20), that is, by reaction of the iron sulfide with the steam existing in the environment. The amount of H_2S produced would be further burnt by normal reaction with the oxygen carrier to release SO_2, see reaction (17).

The conclusion obtained after these tests revealed that the CLC unit must be operated at ϕ values higher than 1.5 to obtain full combustion of H_2S to SO_2 in the FR, and therefore to avoid iron sulfides formation and SO_2 emissions at the AR outlet stream.

Finally, in tests Fe10 and Fe11 the CO_2 used as balance in the previous tests was replaced by N_2. The results obtained during test Fe10 indicated that the gas atmosphere had no influence over the combustion process and sulfur distribution behavior. Test Fe11 was performed without H_2S feeding in a N_2 atmosphere to check if the oxygen carrier particles maintained their reactivity after iron sulfides formed during test Fe8 and later regeneration. The results obtained during this new reference test were very satisfactory considering that almost full CH_4 combustion was again achieved.

3.2.3 Sulfur mass balance

With the above experimental data, a sulfur mass balance was carried out to the different sour gas combustion tests. Figure 10 shows this balance expressed in terms of molar percentage of sulfur considering the amounts released as SO_2 both in the FR and in the AR. It can be observed that in tests Fe2-Fe4 and Fe6-Fe7, all the sulfur detected appeared as SO_2 in the FR, and the mass balances closed within 8 % of deviation. This deviation could be due to experimental errors or to some sulfur accumulation in the oxygen carrier particles as iron sulfides. Only in test Fe8, corresponding to a very low oxygen-carrier-to fuel ratio (ϕ = 1.3), some SO_2 was detected in the AR. Furthermore, during this test the total amount of sulfur detected in the gas phase was lower than in the previous tests. This result would indicate a zone of operating conditions which favored the formation of iron sulfides. Finally, in tests Fe9 and Fe10, more amount than the corresponding to the sulfur fed was obtained at the outlet of the FR, which indicated the regeneration of the oxygen carrier by the disappearance of the iron sulfides formed.

3.2.4 Characterization of the oxygen carrier

Different samples of the Fe20γAl oxygen carrier were extracted from the FR and AR during the 20 hours of continuous operation for further solid characterization. Table 4 shows the main characteristics of those samples.

Powder XRD patterns showed the main crystalline phases existing in the fresh and used samples extracted from the AR at different times of operation. The fresh material was composed by Fe_2O_3 and α-Al_2O_3, and this structure was maintained along operation. Iron sulfides were not detected in any case, which could be due to the detection limit of the apparatus. To evaluate the presence of sulfur inside the samples, used particles were subjected to ultimate analyses with a Thermo Flash 1112 analyzer. Sulfur was only detected in the samples extracted after test Fe8 where only the 76 wt.% of the sulfur fed was released in the gas phase, and some SO_2 was detected in the AR. Nevertheless, the amount of sulfur was very low. No sulfur was found in the samples of subsequent tests, which meant that the iron sulfides formed had disappeared and the material was completely regenerated.

570 The presence of sulfur in the Fe-based oxygen carrier particles was also analyzed by SEM-EDX
571 techniques. Figure 11 shows a SEM image of the cross-section of oxygen carrier particles
572 extracted from the CLC unit after test Fe8. The SEM-EDX analysis revealed a small amount of
573 sulfur in the material.
574 Finally, thermogravimetric experiments were performed to fresh and after-used particles in
575 order to determine the initial reactivity of this material and its evolution during operation in the
576 continuous CLC unit. The reduction reactivity of the particles was analyzed using CH_4 as
577 gaseous fuel. As it can be observed in Figure 12, the samples maintained their reactivity after 20
578 hours of operation, even in the presence of H_2S concentrations as high as 15 vol.%.
579

580 **4. Conclusions**

581 A total of 60 hours of continuous operation with sour gas and different H_2S concentrations up to
582 15 vol. % has been carried out in the ICB-CSIC-g1 facility (500 W_{th}), from which 40
583 corresponded to a Cu-based oxygen carrier and 20 hours to a Fe-based material.
584 During the sour gas combustion tests with the Cu14γAl material, stable operation was achieved
585 with no agglomeration problems. This oxygen carrier was able to burn completely a synthetic
586 sour gas. Sulfur was mainly released as SO_2 in the FR, although some amounts were also
587 released in the AR. As a general rule, the SO_2 concentration in the AR decreased as higher was
588 the oxygen carrier-to-fuel ratio, ϕ. Nevertheless, with the operating conditions selected during
589 this experimental work it was not possible to reach in this reactor SO_2 emissions lower than 200
590 mg/Nm^3, the EU limit of emissions for boilers higher than 200 MW_{th}. Furthermore, Cu_2S was
591 formed at all operating conditions, being accumulated during operation. Therefore, it was
592 concluded that Cu-based oxygen carriers were not adequate for sour gas combustion in a CLC
593 process.
594 On the contrary, the behavior of the Fe-based oxygen carrier during the sour gas combustion
595 tests was very satisfactory. The Fe20γAl material was able to burn completely the sour gas at
596 usual oxygen-carrier-to fuel ratios. The high reactivity of the fresh material was maintained

597 throughout all the operation time even in the presence of high H_2S concentrations. Furthermore,
598 neither SO_2 was released in the AR nor iron sulfides were formed at oxygen carrier-to-fuel
599 ratios higher than 1.5. Therefore, it is concluded that this Fe-based material is very adequate for
600 the combustion of sour gas, even with high H_2S content, allowing CO_2 capture without any SO_2
601 emissions to the atmosphere.
602
603
604
605 **Acknowledgements**
606 This work has been financed by Shell Global Solutions International B.V. within the frame of
607 the agreement PT22648 signed between Shell Global Solutions International B.V. and Instituto
608 de Carboquímica – Consejo Superior de Investigaciones Científicas (ICB –CSIC).
609

610 **References**

611 Abad, A., García-Labiano, F., de Diego, L.F., Gayán, P., Adánez, J., 2007. Reduction kinetics
612 of Cu-, Ni- and Fe-based oxygen carriers using syngas ($CO+H_2$) for chemical looping
613 combustion. Energy & Fuels. 21, 1843-1853.

614 Abad, A., Adánez, J., Cuadrat, A., García-Labiano, F., Gayán, P., de Diego, L.F., 2011. Kinetics
615 of redox reactions of ilmenite for chemical-looping combustion. Chem. Eng. Sci. 66, 689-
616 701.

617 Adánez, J., Gayán, P., Celaya, J., de Diego, L.F., García-Labiano, F., Abad, A., 2006.
618 Chemical-looping combustion in a 10 kW prototype using a CuO/Al_2O_3 oxygen carrier:
619 effect of operating conditions on methane combustion. Ind. Eng. Chem. Res. 45, 6075–
620 6080.

621 Adánez, J., Abad, A., García – Labiano, F., Gayán, P., de Diego, L.F., 2012. Progress in
622 Chemical Looping Combustion and Reforming Technologies. Progress in Energy and
623 Combustion Science. 38, 215-282.

624 Burgers, W.F.J., Northrop, P.S., Kheshgi, H.S., Valencia, J.A., 2011. Worldwide development
625 potential for sour gas. Energy Procedia. 4, 2178-2184.

626 Cabello, A., Dueso, C., García-Labiano, F., Gayán, P., Abad, A., de Diego, L.F., Adánez, J.
627 2014a. Performance of a highly reactive impregnated Fe_2O_3/Al_2O_3 oxygen carrier with
628 CH_4 and H_2S in a 500 W_{th} CLC unit. Fuel. 121, 117-125.

629 Cabello, A., Abad, A., Gayán, P., de Diego, L.F., García-Labiano, F., Adánez, J., 2014b. Effect
630 of operating conditions and H_2S presence on performance of $CaMg_{0.1}Mn_{0.9}O_{3-\delta}$ perovskite
631 material in CLC. Energy & Fuels. 28, 1262-1274.

632 de Diego, L.F., García-Labiano, F., Adánez, J., Gayán, P., Abad, A., Corbella, B.M., Palacios,
633 J.M., 2004. Development of Cu-based oxygen carriers for chemical-looping combustion.
634 Fuel. 83, 1749-1757.

635 de Diego, L.F., Gayán, P., García-Labiano, F., Celaya, J., Abad, A., Adánez, J., 2005.
636 Impregnated CuO/Al_2O_3 oxygen carriers for chemical-looping combustion: avoiding
637 fluidized bed agglomeration. Energy & Fuels. 19, 1850-1856.

638 de Diego, L.F., García-Labiano, F., Gayán, P., Celaya, J., Palacios, J.M., Adánez, J., 2007.
639 Operation of a 10 kW_{th} chemical-looping combustor during 200 h with a $CuO-Al_2O_3$
640 oxygen carrier. Fuel. 86, 1036-1045.
641 Forero, C.R., Gayán, P., García-Labiano, F., de Diego, L.F., Abad, A., Adánez, J. 2010. Effect
642 of gas composition in chemical-looping combustion with copper-based oxygen carriers:
643 Fate of sulphur. Int J Greenhouse Gas Control. 4, 762-770.
644 García-Labiano, F., de Diego, L.F., Gayán, P., Adánez, J., Abad, A., Dueso, C. 2009. Effect of
645 fuel gas composition in chemical-looping combustion with Ni-based oxygen carriers. 1.
646 Fate of sulphur. Ind Eng Chem Res. 48, 2499-2508.
647 Gayán, P., Pans, M.A., Ortiz, M., Abad, A., de Diego, L.F., García-Labiano, F., Adánez, J.,
648 2012. Testing of a highly reactive impregnated Fe_2O_3/Al_2O_3 oxygen carrier for a SR-CLC
649 system in a continuous CLC unit. Fuel Processing Technology. 96, 37-47.
650 Hammer, G., Lübcke, T., Kettner, R., Pillarella, M.R., Recknagel, H., Commichau, A.,
651 Neumann, H.J., Paczynska-Lahme, B., 2006. Natural Gas. Ullmann's Encyclopedia of
652 Industrial Chemistry. Wiley-VCH, Weinheim.
653 HSC Chemistry 6.1., 2008. Chemical Reaction and Equilibrium Software with Thermochemical
654 Database and Simulation Module. Oututec Research Oy, Pori, Finland.
655 IEA, 2013. International Energy Agency. World Energy Outlook 2013.
656 Jacob, KT., Alcock, C.B., 1975. Thermodynamics of $CuAlO_2$ and $CuAl_2O_4$ and Phase equilibria
657 in the system $Cu_2O-CuO-Al_2O_3$. J Am. Ceram. Soc. 58, 192-195.
658 Jerndal, E., Mattisson, T., Lyngfelt, A., 2006. Thermal analysis of chemical-looping
659 combustion. Chem. Eng Res Des. 84, 795-806.
660 Katz, D.L., Cornell, D., Vary, J.A., Kobayasi, R., Elenbaas, J.R., Poettmann, F.H., Weinaug,
661 C.F., 1959. Handbook of Natural Gas Engineering, McGraw-Hill Book Company, New
662 York.
663 Lallemand, F., Perdu, G., Maretto, C., Weiss, C., Magne-Drisch, J., Lucquin, A.C, 2012.
664 Solutions for the treatment of highly sour gases. Process technologies for the cost-effective

665 treatment of natural gas with high and ultra-high acid gas content. Digital Refining.
666 www.digitalrefining.com/article/1000356.
667 Leion, H., Lyngfelt, A., Johansson, M., Jerndal, E., Mattisson, T., 2008. The use of ilmenite as
668 an oxygen carrier in chemical-looping combustion. Chem. Eng Res Des. 86, 1017-1026.
669 Maddox, R.N., 1974. Gas and Liquid Sweetening, 2nd ed. Campbell Petroleum Series, Norman,
670 OK.
671 Mirfenderski, Y., Sprachmann G., 2013. Chemical-looping combustion of sour gas. Patent
672 2610216.
673 Parker, M.E., Northrop, S., Valencia, J.A., Foglesong, R.E., Duncan, W.T., 2011. CO_2
674 Management at ExxonMobil's Labarge Field, Wyoming, USA. Energy Procedia. 4, 5455-
675 5470.
676 Romano, U., 2007. Encyclopaedia of hydrocarbons. Volume III. New developments: energy,
677 transport, sustainability. Istituto della enciclopedia italiana Fondata da Giovanni Treccani
678 S.p.a.
679 Wang, B., Yan, R., Lee, D.H., Liang, D.T., Zheng, Y., Zhao, H., Zheng, C., 2005.
680 Thermodynamic investigation of carbon deposition and sulphur evolution in chemical
681 looping combustion with syngas. Energy & Fuels. 22, 1012-1020.
682
683

684 **Figure Captions**

685 **Figure 1.** Scheme to deal with sour gases through Chemical Looping Combustion technology.

686 **Figure 2.** Scheme of the ICB-CSIC-g1 facility (500 W_{th}) after modifications made for safe
687 operation with high H_2S concentrations.

688 **Figure 3.** Thermodynamic calculations for the systems CuO/sour gas and $CuAl_2O_4$/sour gas.
689 Sour gas 1 composition: 85 vol.% CH_4-15 vol.% H_2S. Sour gas 2 composition: 99.5 vol.% CH_4-
690 0.5 vol.% H_2S. T = 1073 K.

691 **Figure 4.** Gas composition at the outlet stream from the FR and AR, and sulfur balance
692 corresponding to tests Cu7-9 with the Cu14γAl material.

693 **Figure 5.** Sulfur mass balances for the combustion of sour gas with the Cu-based oxygen
694 carrier. Only gas emissions as SO_2 in FR and AR are considered.

695 **Figure 6.** SEM-EDX image of a cross-section of a Cu14γAl oxygen carrier particle after 40 h of
696 sour gas combustion in the CLC unit.

697 **Figure 7.** Reduction reactivity of the Cu14-γAl material after different combustion tests with
698 sour gas. Reducing gas: 15 vol.% CH_4. T = 1073 K.

699 **Figure 8.** Thermodynamic calculations for the systems Fe_2O_3-Fe_3O_4/sour gas (a) and
700 Fe_2O_3 (Al_2O_3)-$FeO{\cdot}Al_2O_3$/sour gas (b). Sour gas composition: 85 vol.% CH_4-15 vol.% H_2S.
701 T = 1223K.

702 **Figure 9.** Gas composition at the outlet stream from the FR and AR, and sulfur balance
703 corresponding to tests Fe5-9 with the Fe20γAl oxygen carrier.

704 **Figure 10.** Sulfur mass balances for the combustion of sour gas with the Fe-based oxygen
705 carrier.

706 **Figure 11.** SEM-EDX image of a cross-section of a Fe20γAl oxygen carrier particle after test
707 Fe8 in the CLC unit.

708 **Figure 12.** Reduction reactivity of the Fe20γAl oxygen carrier during the combustion tests with
709 sour gas. Reducing gas: 15 vol.% CH_4. T = 1223 K.

710

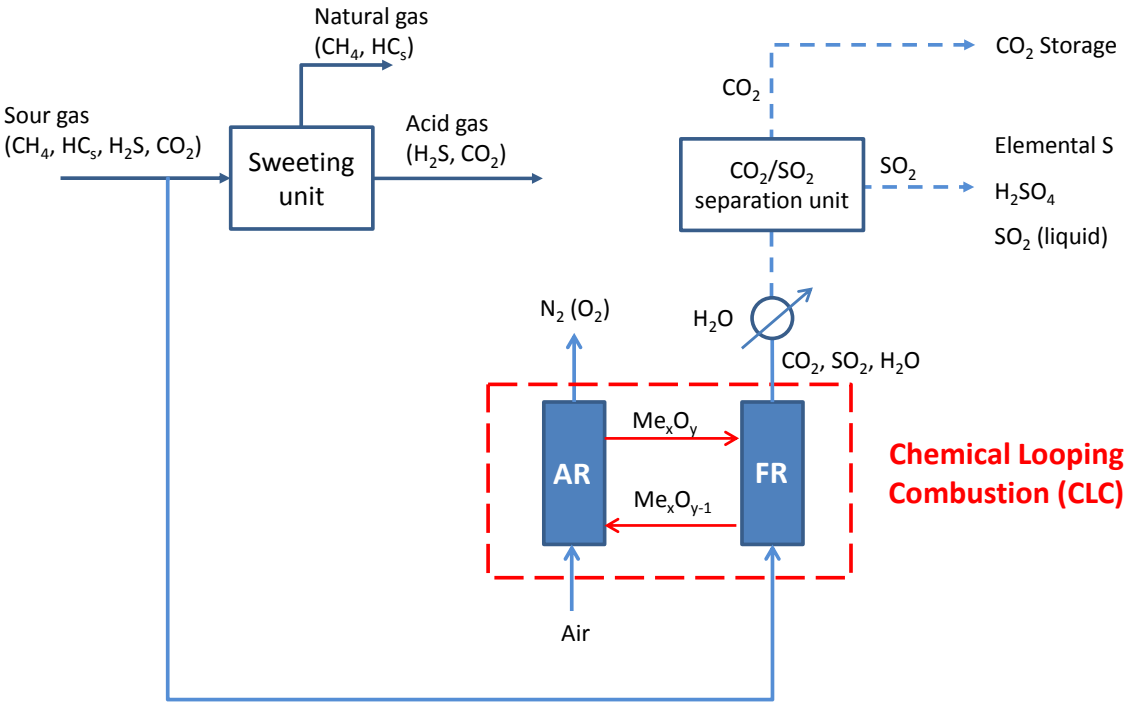

Figure 1. Scheme to deal with sour gases through Chemical Looping Combustion technology.

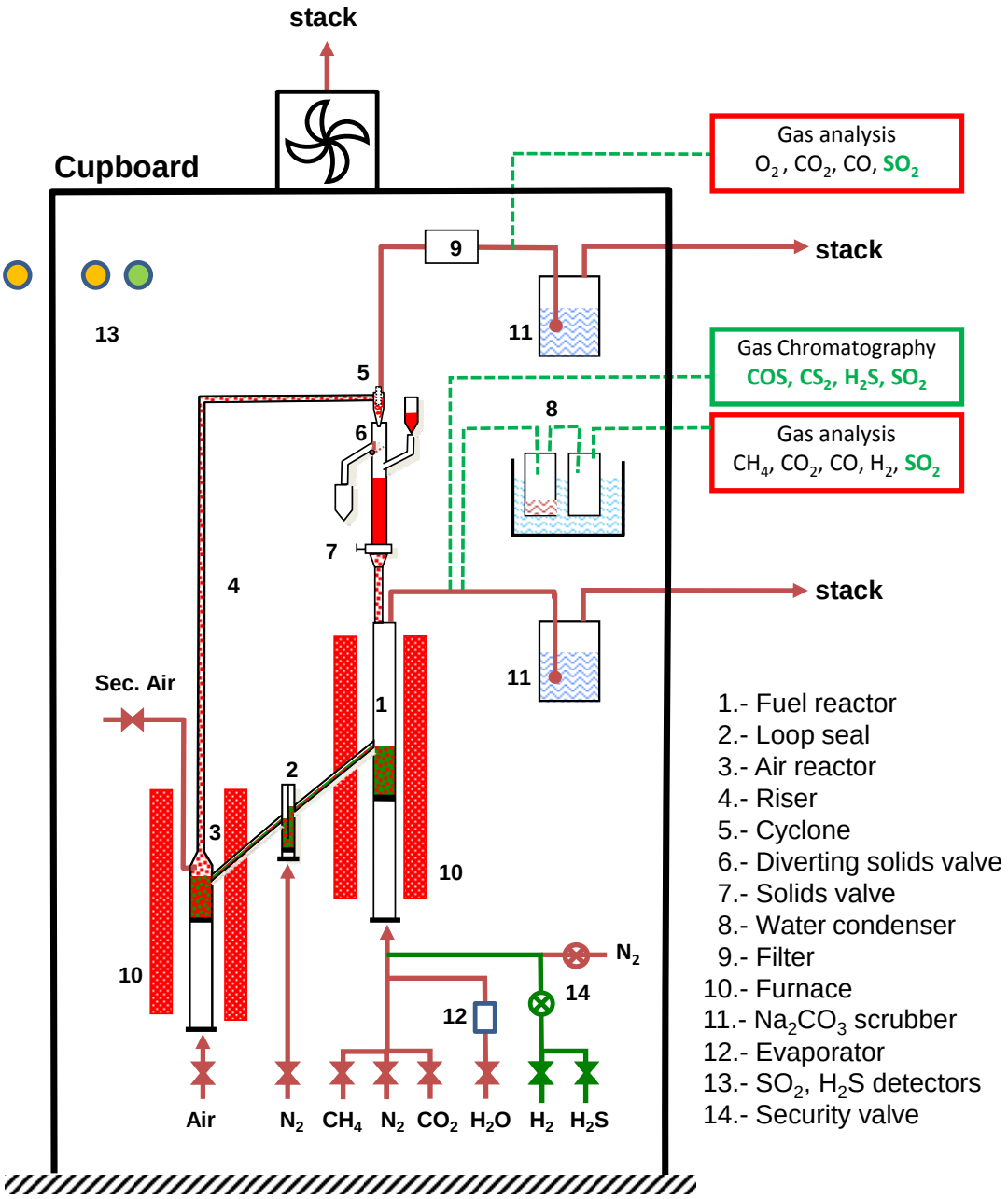

Figure 2. Scheme of the ICB-CSIC-g1 facility (500 W_{th}) after modifications made for safe operation with high H_2S concentrations.

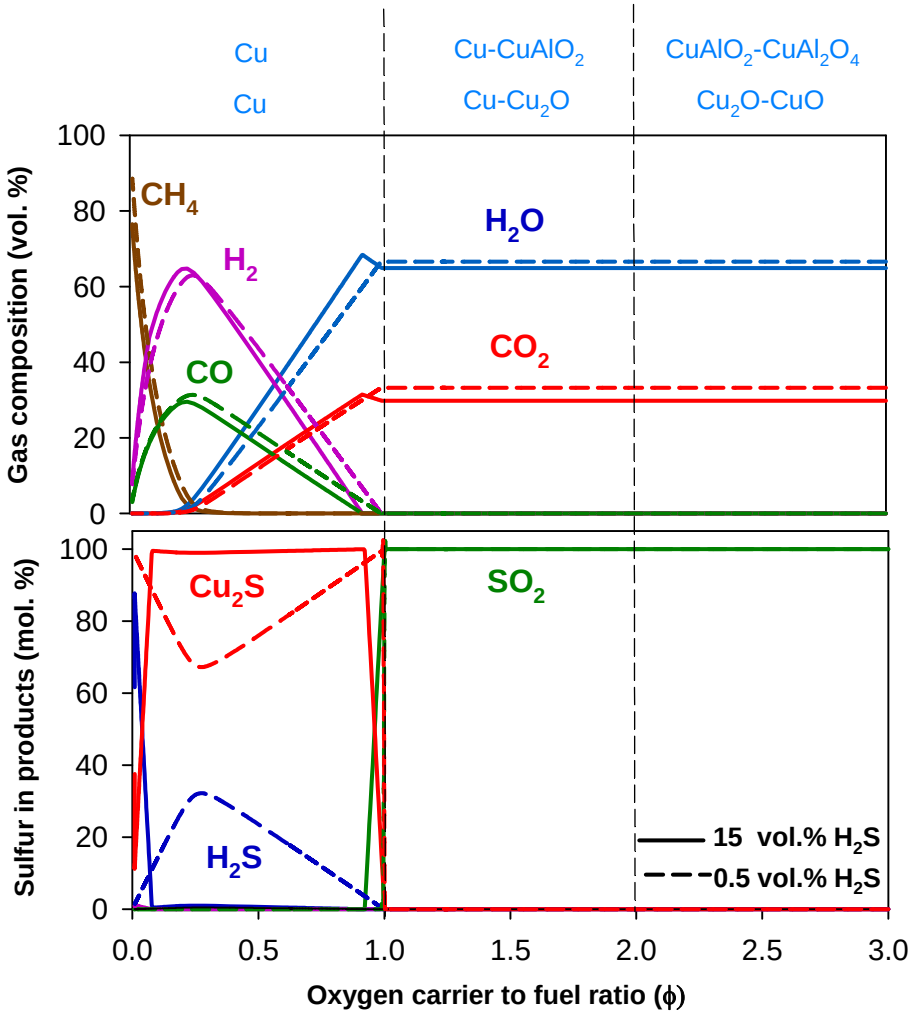

Figure 3. Thermodynamic calculations for the systems CuO/sour gas and $CuAl_2O_4$/sour gas. Sour gas 1 composition: 85 vol.% CH_4-15 vol.% H_2S. Sour gas 2 composition: 99.5 vol.% CH_4-0.5 vol.% H_2S. T = 1073 K.

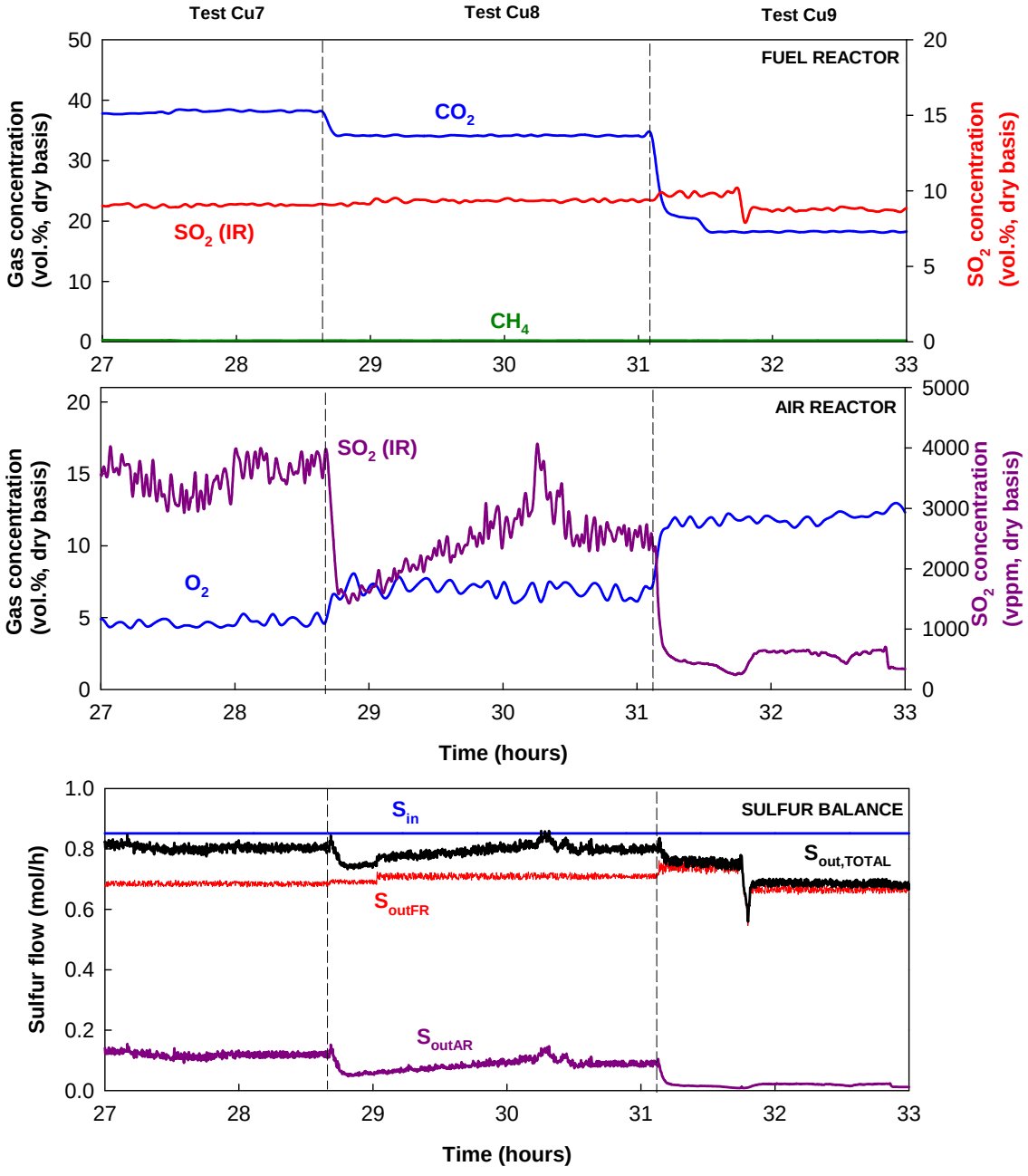

Figure 4. Gas composition at the outlet stream from the FR and AR, and sulfur balance corresponding to tests Cu7-9 with the Cu14γAl material.

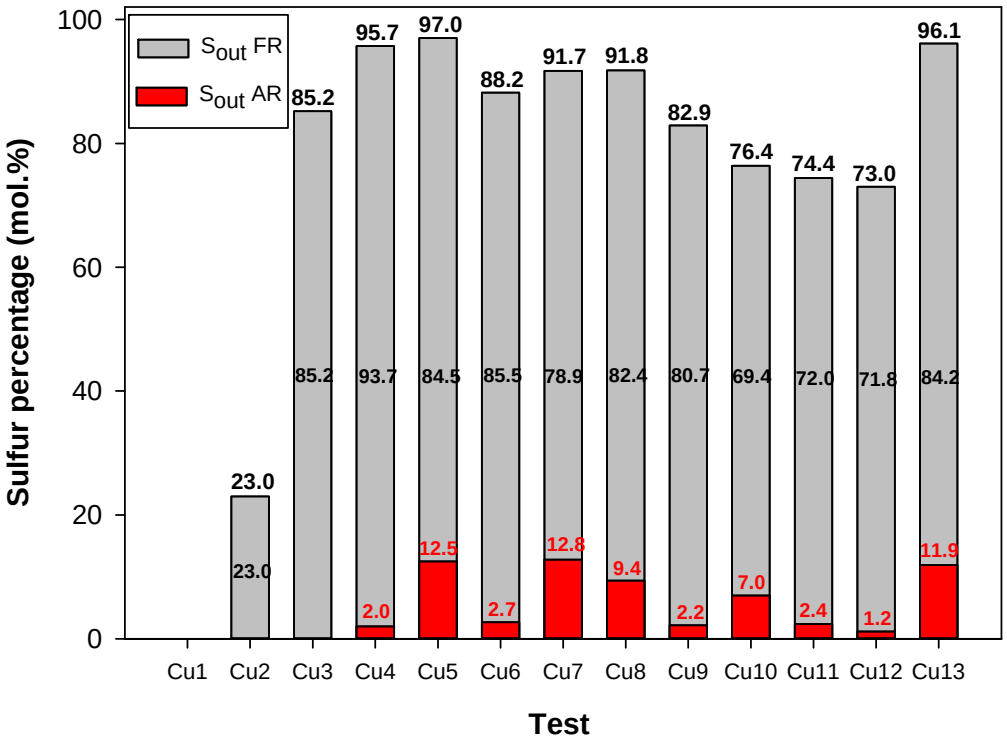

Figure 5. Sulfur mass balances for the combustion of sour gas with the Cu-based oxygen carrier. Only gas emissions as SO_2 in FR and AR are considered.

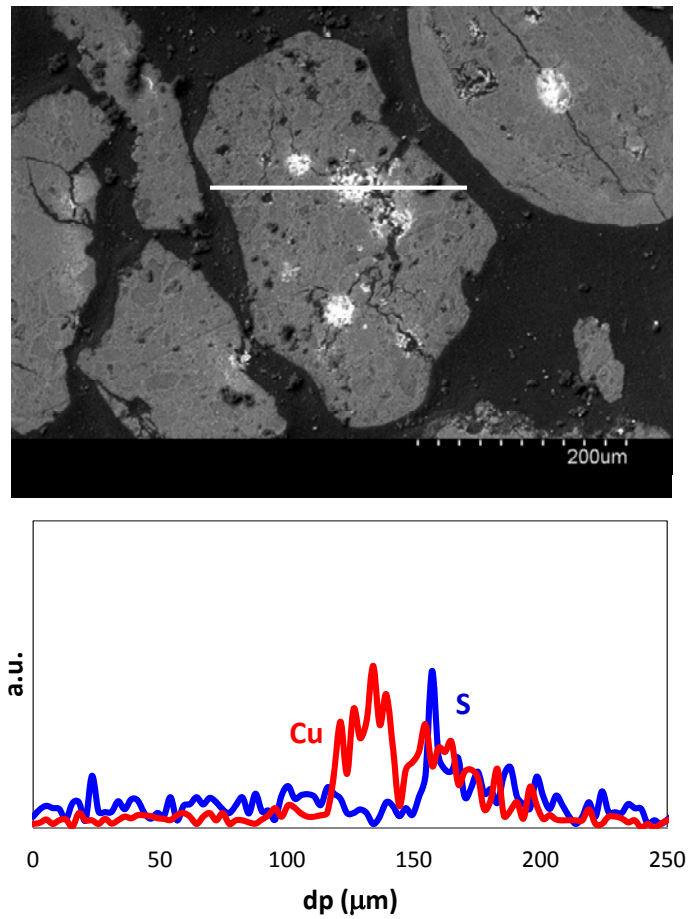

Figure 6. SEM-EDX image of a cross-section of a Cu14γAl oxygen carrier particle after 40 h of sour gas combustion in the CLC unit.

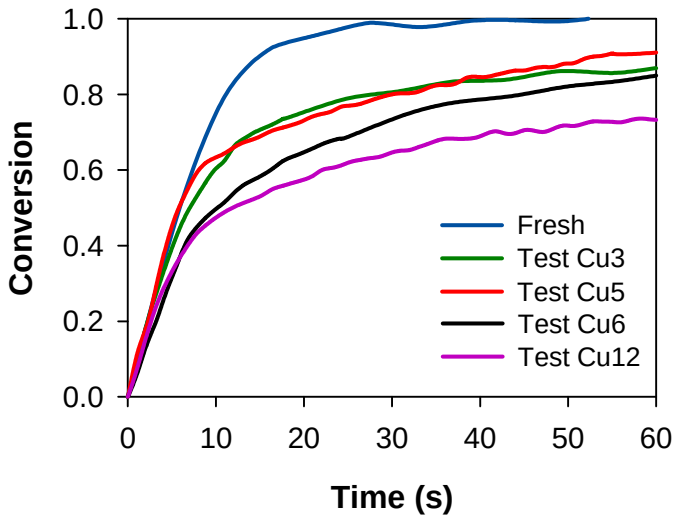

Figure 7. Reduction reactivity of the Cu14-γAl material after different combustion tests with sour gas. Reducing gas: 15 vol.% CH_4. T = 1073 K.

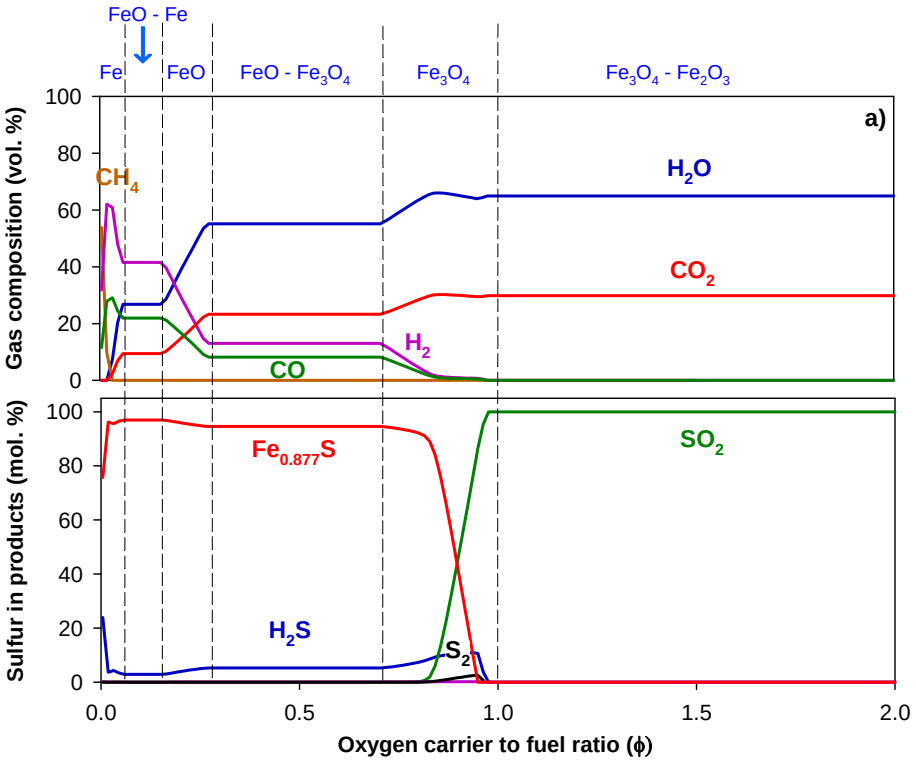

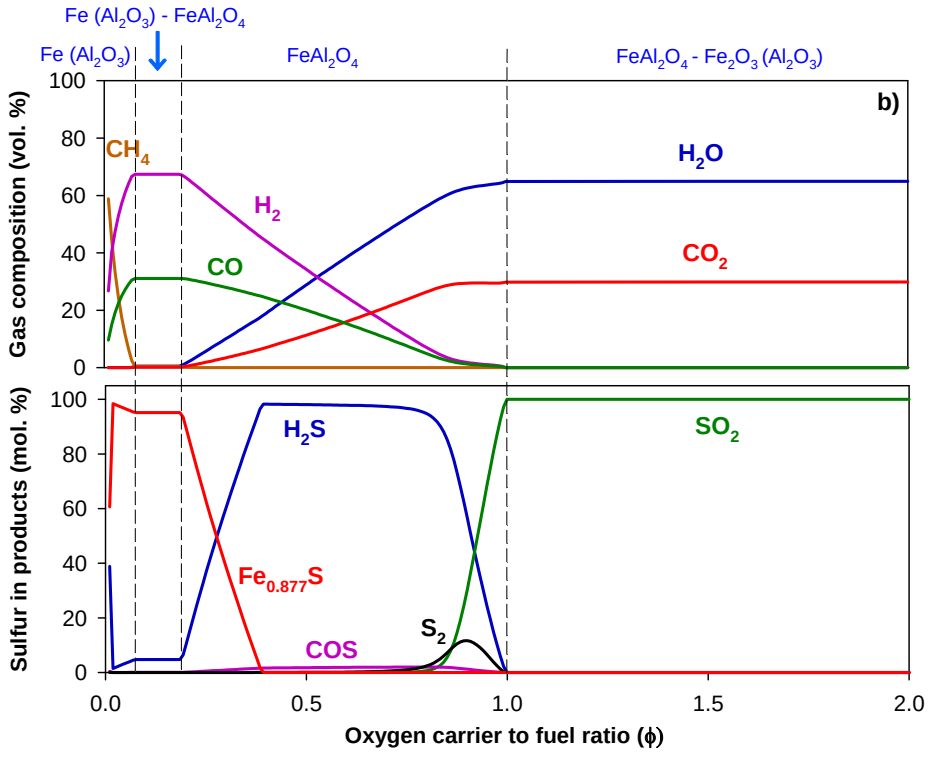

Figure 8. Thermodynamic calculations for the systems Fe_2O_3-Fe_3O_4/sour gas (a) and Fe_2O_3 (Al_2O_3)-$FeO{\cdot}Al_2O_3$/sour gas (b). Sour gas composition: 85 vol.% CH_4-15 vol.% H_2S. T = 1223 K.

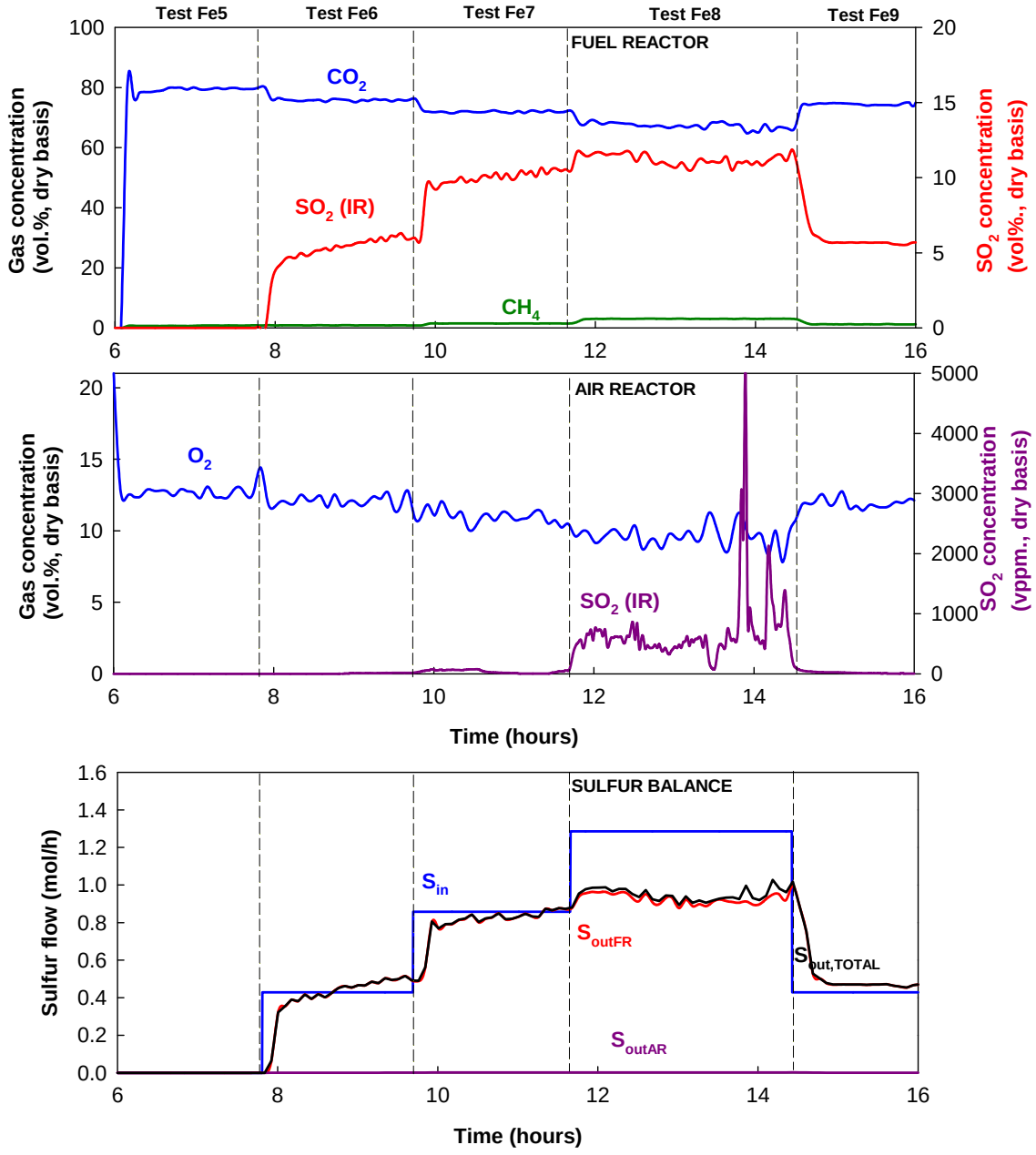

Figure 9. Gas composition at the outlet stream from the FR and AR, and sulfur balance corresponding to tests Fe5-Fe9 with the Fe20γAl oxygen carrier.

.

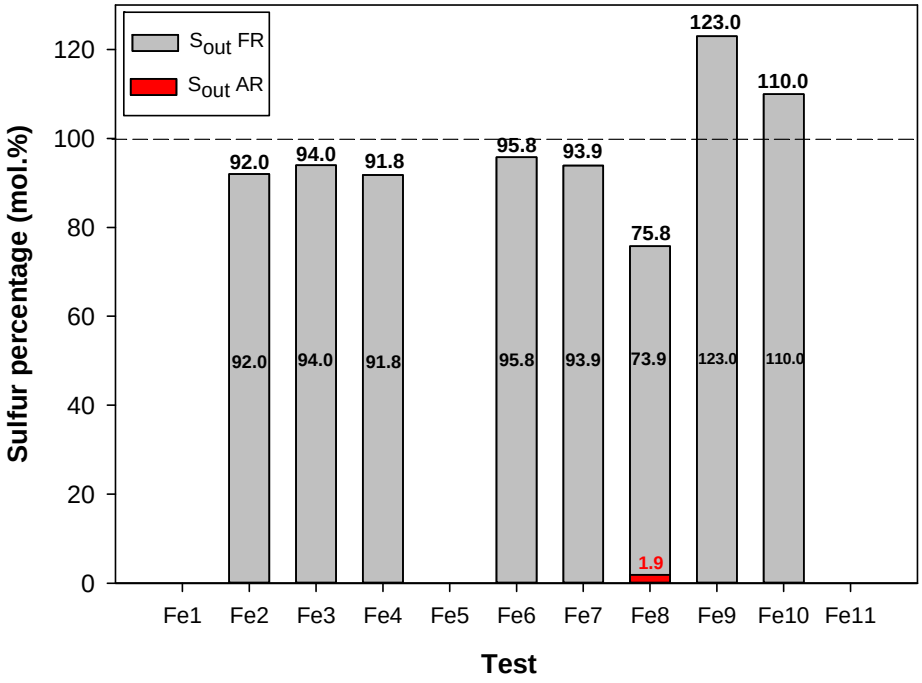

Figure 10. Sulfur mass balances for the combustion of sour gas with the Fe-based oxygen carrier.

807

808

809

810

811

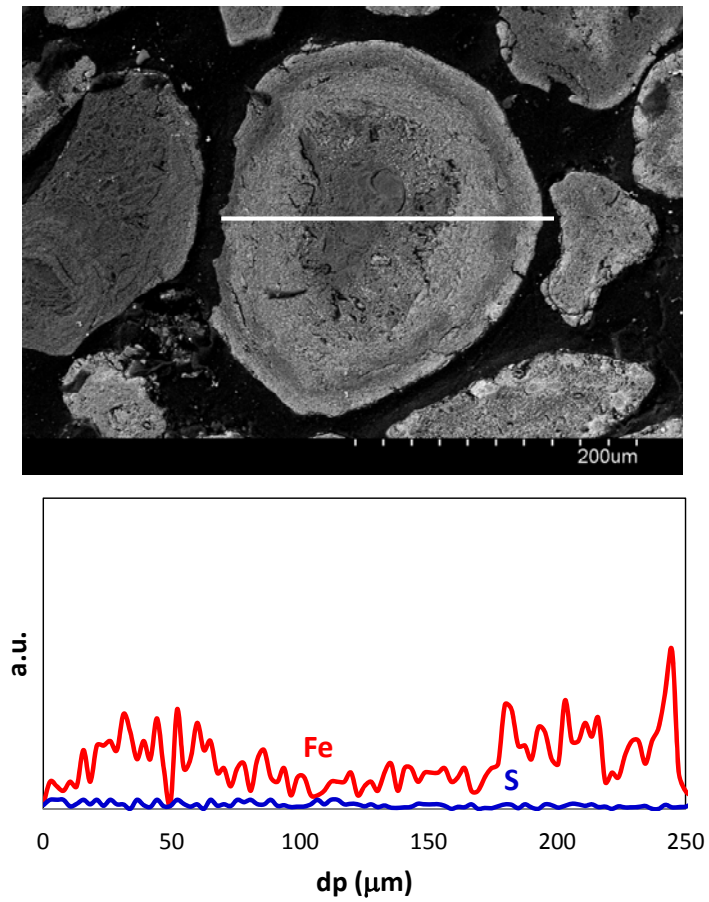

812

813 **Figure 11.** SEM-EDX image of a cross-section of a Fe20γAl oxygen carrier particle after test

814 Fe8 in the CLC unit.

815

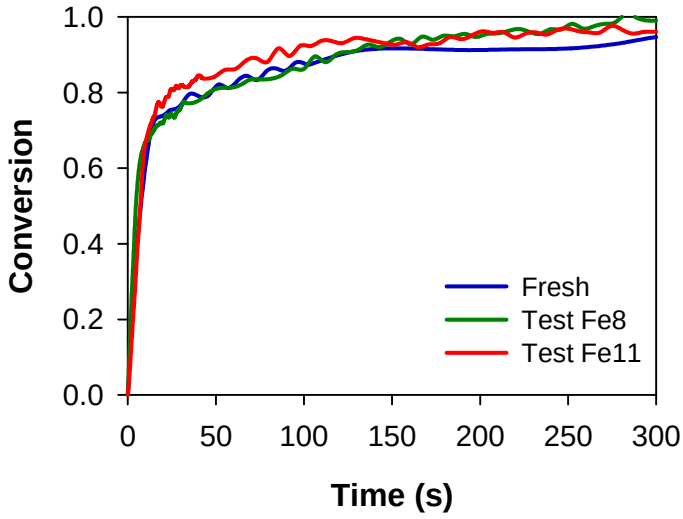

Figure 12. Reduction reactivity of the Fe20γAl oxygen carrier during the combustion tests with sour gas. Reducing gas: 15 vol.% CH_4. T = 1223 K.

Tables

837

838

839

840

841

842

843 **Table 1.** Combustion tests of sour gas with the Cu-based oxygen carrier.

Test	T_{FR} (K)	T_{AR} (K)	Gas composition (vol. %)						f_s (kg/h)	ϕ	Time (h)	Accumulated time (h)
			CH_4	H_2	H_2O	H_2S	N_2	CO_2				
Cu1	1073	1123	30	5	10	0	55	0	14.7	2.4	2.0	2.0
Cu2	1073	1123	30	5	10	0.3	54.7	0	9.4	1.5	3.0	5.0
Cu3	1073	1123	30	5	10	1	54	0	9.4	1.4	4.0	9.0
Cu4	1073	1123	30	5	10	3	52	0	9.7	1.3	9.5	18.5
Cu5	1073	1123	30	5	10	5	50	0	9.5	1.3	5.0	23.5
Cu6	1073	1123	20	5	10	5	60	0	9.5	1.9	3.5	27.0
Cu7	1073	1123	30	5	10	10	45	0	9.2	1.3	1.5	28.5
Cu8	1073	1123	25	5	10	10	50	0	9.2	1.5	2.5	31.0
Cu9	1073	1123	15	5	10	10	60	0	9.2	2.5	2.0	33.0
Cu10	1073	1123	20	5	10	15	50	0	9.4	1.8	2.5	35.5
Cu11	1073	1123	15	5	10	15	55	0	9.4	2.4	2.5	38.0
Cu12	1073	1123	10	5	10	15	60	0	9.4	3.7	2.0	40.0
Cu13[a]	1073	1123	30	5	10	5	0	50	9.4	1.3	3.0	3.0

844 [a.] New batch of Cu-based material.

845

Table 2. Combustion tests of sour gas with the Fe-based oxygen carrier.

Test	T_{FR} (K)	T_{AR} (K)	Gas composition (vol. %)						f_s (kg/h)	ϕ	Time (h)	Accumulated time (h)
			CH_4	H_2	H_2O	H_2S	N_2	CO_2				
Fe1	1173	1223	10	5	20	0	0	65	14.0	4.4	1.5	1.5
Fe2	1173	1223	10	5	20	5	0	60	14.0	3.3	1.5	3.0
Fe3	1173	1223	10	5	20	10	0	55	14.0	2.6	2.0	5.0
Fe4	1173	1223	10	5	20	15	0	50	14.0	2.2	2.0	7.0
Fe5	1173	1223	20	5	20	0	0	55	13.0	2.1	2.0	9.0
Fe6	1173	1223	20	5	20	5	0	50	13.0	1.7	2.0	11.0
Fe7	1173	1223	20	5	20	10	0	45	13.0	1.5	2.0	13.0
Fe8	1173	1223	20	5	20	15	0	40	13.0	1.3	2.5	15.5
Fe9	1173	1223	20	5	20	5	0	50	13.0	1.7	1.5	17.0
Fe10	1173	1223	20	5	20	5	50	0	13.0	1.7	1.5	18.5
Fe11	1173	1223	10	5	20	0	65	0	13.0	3.9	1.5	20.0

854

855

856

857

858

859 **Table 3.** Main characteristics of fresh and after-used particles of the Cu14-γAl material.

Test	H_2S (vol.%)	Time (h)	S[a] (wt.%)	Cu_2S[b] (wt.%)	XRD (AR samples)
Fresh					γ-Al_2O_3, $CuAl_2O_4$, CuO
Cu1	0	2.0			
Cu2	0.3	5.0	0.25	1.23	γ-Al_2O_3, δ-Al_2O_3, $CuAl_2O_4$, CuO
Cu3	1	9.0			
Cu4	3	18.5	0.23	1.14	γ-Al_2O_3, δ-Al_2O_3, α-Al_2O_3, $CuAl_2O_4$, CuO
Cu5	5	23.5			
Cu6	5	27.0	0.33	1.63	γ-Al_2O_3, δ-Al_2O_3, α-Al_2O_3, $CuAl_2O_4$, CuO
Cu7	10	28.5			
Cu8	10	31.0			
Cu9	10	33.0	0.40	1.98	γ-Al_2O_3, δ-Al_2O_3, α-Al_2O_3, $CuAl_2O_4$, CuO
Cu10	15	35.5			
Cu11	15	38.0			
Cu12	15	40.0	0.38	1.88	γ-Al_2O_3, δ-Al_2O_3, α-Al_2O_3, $CuAl_2O_4$, CuO

860 [a] Determined by ultimate analysis

861 [b] Calculated from a.

862

Table 4. Main characteristics of fresh and after-used particles of the Fe20γAl oxygen carrier.

	Gas composition (vol.%)			
Test	CH_4	H_2S	S (wt. %)[a]	XRD (AR samples)
Fresh				α-Al_2O_3, Fe_2O_3
Fe1	10	0		
Fe2	10	5		
Fe3	10	10		
Fe4	10	15	0.00 (0.00)	α-Al_2O_3, Fe_2O_3
Fe5	20	0		
Fe6	20	5		
Fe7	20	10		
Fe8	20	15	0.02 (0.02)	α-Al_2O_3, Fe_2O_3
Fe9	20	5		
Fe10	20	5		
Fe11	10	0	0.00 (0.00)	α-Al_2O_3, Fe_2O_3

a. Determined by ultimate analysis. Data from FR in brackets.